Robustness of entropy plateaus: A case study of triangular Ising antiferromagnets

Owen Bradley, Chunhan Feng, Richard T. Scalettar, and Rajiv R. P. Singh
Department of Physics, University of California, Davis, California 95616, USA

(Received 31 January 2019; revised manuscript received 26 July 2019; published 20 August 2019)

Residual entropy is a key feature associated with emergence in many-body systems. From a variety of frustrated magnets to the onset of spin-charge separation in Hubbard models and fermion-Z_2-flux variables in Kitaev models, the freezing of one set of degrees of freedom and the establishment of local constraints are marked by a plateau in entropy as a function of temperature. Yet, with the exception of the rare-earth pyrochlore family of spin-ice materials, evidence for such plateaus is rarely seen in real materials, raising questions about their robustness. Following recent experimental findings of the absence of such plateaus in the triangular-lattice Ising antiferromagnet (TIAF) $TmMgGaO_4$ by Li *et al.*, we explore in detail the existence and rounding of entropy plateaus in TIAF. We use a transfer-matrix method to numerically calculate the properties of the system at different temperatures and magnetic fields, with further neighbor interactions and disorder. We find that temperature windows of entropy plateaus exist only when second-neighbor interactions are no more than a couple of percent of the nearest-neighbor ones, and they are also easily destroyed by disorder in the nearest-neighbor exchange variable, thereby explaining the challenge in observing such effects.

DOI: 10.1103/PhysRevB.100.064414

I. INTRODUCTION

Residual entropy is a hallmark of frustrated systems, reflecting the emergence of local constraints or new degrees of freedom distinct from the microscopic ones [1]. One of the earliest theoretical works in this direction was the calculation of residual entropy associated with the establishment of ice rules in water done by Pauling [2]. It is now well established that such a strongly constrained phase has an analog in magnetic systems known as spin-ice [3–5]. Such a classical spin-liquid exhibits residual entropy [6–8] and supports magnetic-monopole excitations. Quantum fluctuations in such a system can lead to a highly resonating quantum spin-liquid phase with emergent quantum electrodynamics.

In models of geometrically frustrated magnets, such residual entropy is widespread [9]. But, how robust are they in real materials? In fact, the issue is much broader than geometric frustration. In recent years, there has been a lot of interest in Kitaev materials [10–14]. At a microscopic level, the honeycomb-lattice Kitaev model describes spins interacting with anisotropic bond-direction-dependent exchange interactions [15]. Yet, the model can be exactly mapped onto one of the Majorana fermions and Z_2-valued fluxes. As the fermions reach their degeneracy temperature or freeze-out if they have a gapped spectrum, an entropy plateau sets in [16]. Indeed, some hints of entropy plateaus have been seen in experiments [17,18]. The plateaus are far more robust than the soluble models. For example, spin-S models show even more interesting possibilities of entropy plateaus [19–22]. When Kitaev couplings are the same along all three axes, there are incipient plateaus at an entropy of $\ln(2S+1)/2$, which keeps increasing with spin S. The physical mechanism behind such large entropy values at the plateau with increasing S is not well understood.

Entropy plateaus are also a prominent feature of correlated electron Hamiltonians such as the Hubbard and periodic Anderson models [23–25]. In the regime of strong on-site interaction U, there are clearly distinct charge and spin energy scales. At the higher scale, $T \sim U$, a drop in entropy occurs when doubly occupied sites are frozen out. At the lower scale, $T \sim J = 4t^2/U$, a second drop occurs that is associated with the development of antiferromagnetic (AF) correlations. Studies of the specific heat $C(T)$ in one dimension [26–28], and in infinite dimensions, i.e. within dynamical mean-field theory (DMFT) [29–31], suggested the disappearance of an entropy plateau as $U \to t$, and hence the two energy scales merge. However, quantum Monte Carlo calculations for the half-filled Hubbard model on a two-dimensional square lattice revealed that the two-peak structure in $C(T)$ is robust, surviving even down to $U \sim t$. An interesting feature of this robustness was an apparent interchange in the "driving force" of the entropy reduction. At strong U, changes in the *potential energy* led to the high-T specific-heat peak, while at small U it is the changes in the *kinetic energy* that yield the peak at higher temperature.

Preservation of the entropy plateaus in these systems appears to be linked to the AF order. On a honeycomb lattice [32], the two peaks in $C(T)$ merge as U is reduced, with a resultant destruction of the plateau. The most natural explanation is that, unlike the square lattice where antiferromagnetism exists down to $U = 0$, the honeycomb lattice has a quantum critical point $U_c/t \sim 4$, below which antiferromagnetism disappears [25,33].

The Ising antiferromagnet on the triangular lattice is an iconic problem in frustrated magnetism where an exact residual ground-state entropy was first calculated by Wannier [34,35]. Several materials, including $CeCd_3As_3$ [36], FeI_2 [37], and $TmMgGaO_4$ [38,39], have been identified

 ©2019 American Physical Society

experimentally as triangular-lattice Ising antiferromagnet (TIAF) systems due to the strong Ising nature of their constituent spins. Despite being of such central interest, there are few (or no) experimental systems where such residual entropy has been observed. Very recently, Li *et al.* [39] investigated the triangular-lattice Ising antiferromagnetic material $TmMgGaO_4$. They measured the heat capacity and entropy of the system as well as the magnetization as a function of an applied magnetic field. Li *et al.* found a complete absence of entropy plateaus and rounded magnetization plateaus, with roundings that are only partly thermal and partly reflect the presence of quenched impurities.

The TIAF has been studied over the years using a variety of analytical and numerical methods. Such studies have determined the phase diagram, minimum energy spin configurations, as well as entropy and specific-heat curves for finite-size clusters [40–45]. Several numerical studies of disordered TIAF (and ferromagnetic) systems have also been performed, including investigations of random site vacancies, diluted lattices, varying bond lengths, and disorder in the applied field [46–48].

The purpose of this paper is to explore the rounding or absence of entropy and magnetization plateaus in the TIAF as a function of applied field due to further neighbor interactions and disorder. How large a perturbation can the system tolerate before the plateaus disappear altogether? We use a numerical transfer-matrix-based approach to calculate the thermodynamic properties. We first confirm that, in the absence of second-neighbor interactions, the magnetization of the pure TIAF jumps from 0 to 1/3 in an infinitesimal field, and then at a field of $B = 6$ it jumps again to full saturation value. The transition field $B = 6$ also has a finite ground-state entropy.

We next consider antiferromagnetic second-neighbor interactions, as appropriate for the $TmMgGaO_4$ material. This interaction is shown to lead to a striped ground-state phase and a finite-temperature phase transition. The entropy plateaus are lost rapidly with a fairly small second-neighbor interaction of only a few percent. They are replaced by sharp drops in the entropy at a first-order transition. This is in contrast to the spin-ice system, where the entropy plateaus are very robust and survive even with long-range dipolar interactions [3–5] and quantum fluctuations [49]. If we consider only the nearest-neighbor TIAF with disorder in the exchange interactions, rounded entropy plateaus are quickly destroyed.

When the second-neighbor interaction is about 10% of the nearest-neighbor value, there are magnetization plateaus at values 0, 1/3, 1/2, and 1. Thermal rounding of the magnetization plateaus is very gradual. Despite the finite temperature, the plateaus remain extremely flat, reflecting the energy gap in the system. The rounding is much stronger with quenched disorder. We find that strong disorder is needed to obtain results that look quantitatively like the experiments, with both plateaus at magnetizations of 1/3 and 1/2 becoming significantly rounded.

The plan of the paper is as follows: First, an overview of the model and the numerical methods is given. We then present entropy $S(T)$ and specific-heat $C(T)$ results for the TIAF system with no magnetic field present, in the absence of any disorder, for various strengths of the second-nearest-neighbor interaction J_2. Disorder in the nearest-neighbor interaction J_1 is then introduced, and we study its influence on entropy plateaus in the TIAF. We then show the influence of an applied magnetic field on the form of $S(T)$ and $C(T)$, and we present magnetization curves for various temperatures and J_2 values. Our final set of results shows the effect of quenched disorder in both J_1 and J_2 on the magnetization plateaus observed in the TIAF. Two disorder types—box and Gaussian—are compared. We finally present our conclusions.

II. MODEL AND METHODS

We study a triangular lattice of Ising spins. Both nearest-neighbor (NN) and next-nearest-neighbor (NNN) interactions are considered in an applied magnetic field B, perpendicular to the plane of the lattice. The Hamiltonian studied is thus given by

$$H = -J_1 \sum_{\langle i,j\rangle} S_i S_j - J_2 \sum_{\langle\langle i,j\rangle\rangle} S_i S_j - B \sum_i S_i, \qquad (1)$$

where J_1 and J_2 denote the NN and NNN coupling strengths, respectively, and $S_i = \pm 1$ is the Ising spin at site i of the lattice, which may be aligned parallel or antiparallel to the applied field. The first sum is taken over all pairs of NN sites, and the second is a sum over all NNN pairs. Negative values of J_1 and J_2 correspond to antiferromagnetic interactions.

We employ a transfer-matrix approach to obtain values of the Helmholtz free energy $F(T, B)$ for our TIAF system, which is found from the largest eigenvalue of a suitably constructed transfer matrix. We consider a long cylinder-geometry for our calculations, which implies periodic boundary conditions in the short direction. The second-neighbor interactions demand that the transfer matrix involve two rows of spins at a time. This is no longer an analytically soluble problem. It also limits the sizes of systems that can be studied. Furthermore, in order for the system to have compatibility with a three-sublattice structure of the triangular lattice, and for our results not to be artificially affected by the periodic boundary conditions in the short direction, we need to have a multiple of three spins in each row. Our results are all based on six spins in a row, which requires a $2^{12} \times 2^{12}$ transfer matrix. We believe that these results should be reasonably close to the thermodynamic limit, except near phase transitions or points where the correlation length becomes large. For the nearest-neighbor Ising model in zero field, the calculated entropy curves are close, though clearly not identical, to the exact answer.

Since the TIAF with nearest- and second-neighbor interactions shows a first-order phase transition over a range of parameters, with a jump in the entropy of the system [45], there will be large finite-size effects near the transition. In a finite system, all thermodynamic functions must be analytic and hence no jump in entropy is possible. Instead, one would have a rounded δ-function in the heat capacity per site, whose peak for an $L \times L$ system scales as L^2 and peak-width scales as $1/L^2$. In the thermodynamic limit, this becomes a δ-function, whose integral gives a jump in the entropy, per site, at the transition.

In an $L \times \infty$ transfer-matrix calculation also the largest eigenvalue of the transfer matrix must be analytic at any finite temperature and hence there can be no jump in a thermodynamic property. The correlation length in the infinite direction must be finite (set by L) and the jump in entropy must be rounded over a range of temperatures near the transition. Since the linear dimension $L = 6$ of our study is much smaller than those studied by Monte Carlo simulations of Rastelli *et al.* [45], the rounding must be over a wider temperature range. However, we would not expect the transition temperature to be strongly size-dependent for a first-order transition, and our conclusions regarding rounding of entropy plateaus at low temperatures should not be affected by this behavior near the transition. Comparing our data with those of Rastelli *et al.* will allow us to quantify this effect.

Previous Monte Carlo data [45] are only available for a magnitude of J_2 greater than or equal to 0.1, which pushes the first-order transition temperature outside the plateau region of the nearest-neighbor model. To accurately evaluate the jump in entropy ΔS for smaller J_2, we have performed further Monte Carlo simulations on up to 96×96 lattices. At small J_2, the transition temperature is very low. The transition is strongly first order, with clear evidence for hysteresis. The internal energy jumps at the transition and ΔE are easily read off from the simulations, as is the transition temperature where the sharp change in energy occurs. At the transition, we know that the two states must have equal free energy. Thus we can get the entropy jump by using the relation $\Delta S = \Delta E / T_c$. These will also be compared with the transfer-matrix calculations.

Free energies per site are found for a range of temperatures (at fixed B), and over a range of magnetic-field values at fixed temperature, from which the thermodynamic properties $S(T)$, $C(T)$, and $M(B)$ can be computed easily by taking suitable derivatives. For a triangular lattice N sites wide, with $2P$ rows of spins (i.e., there are P distinct "blocks" of two rows, each N sites in width), the partition function is given by $Z = \sum_{s_i} e^{-\beta H}$, where H is as given in Eq. (1) and we take k_B equal to unity, with the sum taken over all spin configurations. The method relies on the fact that a careful construction of a particular $2^{2N} \times 2^{2N}$ matrix M allows one to write the partition function as $Z = \sum_{S_A} M^P(S_A; S_A) = \mathrm{Tr}[M^P]$, where S_A is shorthand for a particular configuration of $2N$ spins within a block. The partition function is thus given by

$$Z = \lambda_1^P + \lambda_2^P + \lambda_3^P \dots, \tag{2}$$

where λ_i are the eigenvalues of the transfer matrix M. Taking λ_1 to be the maximum eigenvalue, we have that

$$Z = \lambda_1^P \left[1 + \left(\frac{\lambda_2}{\lambda_1} \right)^P + \left(\frac{\lambda_3}{\lambda_1} \right)^P + \cdots \right], \tag{3}$$

and so in the limit $P \to \infty$ (i.e., for a semi-infinite triangular lattice) we have that $Z = \lambda_1^P$. The free energy is found via $F = -T \ln Z = -T \ln(\lambda_1^P) = -TP \ln(\lambda_1)$. Since the total number of sites is $N_{\mathrm{tot}} = 2P \times N$, the free energy per site is given by

$$f = \frac{F}{N_{\mathrm{tot}}} = \frac{-T \ln(\lambda_1)}{2N}. \tag{4}$$

With this method, we also investigate the influence of disorder in J_1 and J_2. To obtain the partition function when disorder is present, we instead take the trace of the product of many transfer matrices, each one using a different set of values for J_1 and J_2. We show results for which these parameters are chosen from a uniform distribution and also a Gaussian distribution.

III. RESULTS AND DISCUSSION

A. Results in zero field with no disorder

The transfer-matrix method outlined above was used to obtain $S(T)$ and $C(T)$ results for the TIAF in the absence of a magnetic field, with no disorder. To investigate the effect of the NNN coupling, we calculated $S(T)$ and $C(T)$ curves for a range of J_2 values including $J_2 = 0$, i.e., NN interactions only. Figure 1 shows entropy per site as a function of temperature for various antiferromagnetic NNN interaction strengths: $J_2 = 0, -0.01, -0.02, -0.05, -0.10$, and -0.25 (with $J_1 = -1$). As expected, for $J_2 = 0$ (black curve) we observe a nonzero residual entropy as the temperature tends to zero, since frustration in the triangular lattice produces a degenerate ground state when only nearest-neighbor interactions are present. The presence of any nonzero next-nearest-neighbor interaction removes the ground-state degeneracy, giving an entropy that tends to zero at low temperature. For small values of J_2 (e.g., $J_2 = -0.01$), a plateau in the $S(T)$ curve is observed at the value of the residual entropy for the $J_2 = 0$ case, before sharply dropping to $S = 0$ as the temperature reaches zero. As the magnitude of J_2 increases, the entropy plateau is gradually rounded until there is no longer a plateau visible in $S(T)$ (i.e., for $|J_2| \geqslant 0.05$).

Finite-size effects can be seen in the inset of Fig. 1. The entropy function cannot have a jump in a finite system, instead that change in entropy will happen over a range of temperatures. The Monte Carlo study of Rastelli *et al.* [45] allows us

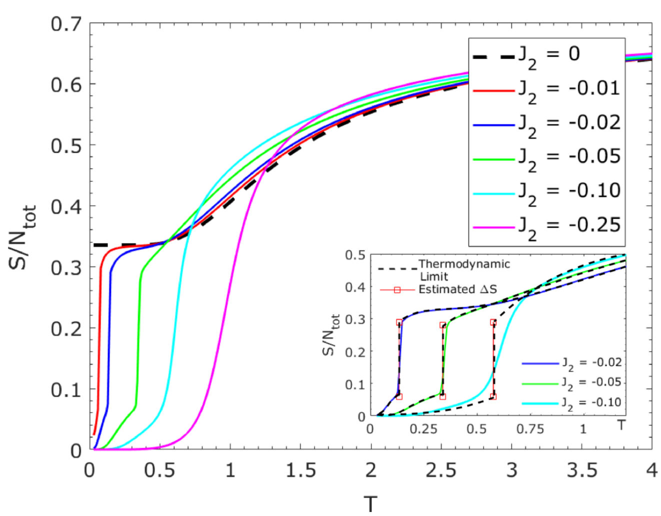

FIG. 1. Entropy per site as a function of temperature for the semi-infinite TIAF geometry, calculated using the transfer-matrix method. $S(T)$ curves are shown for six different values of the NNN interaction J_2, with $J_1 = -1$ fixed. At $J_2 = 0$, a residual ground-state entropy is observed at zero temperature. The inset shows a comparison of our $J_2 = -0.1, -0.05$, and -0.02 entropy functions with the entropy jump expected in the thermodynamic limit. The magnitude of the jump and the transition temperatures are obtained from the hysteresis of the energy function in the Monte Carlo simulations of up to 96×96 systems.

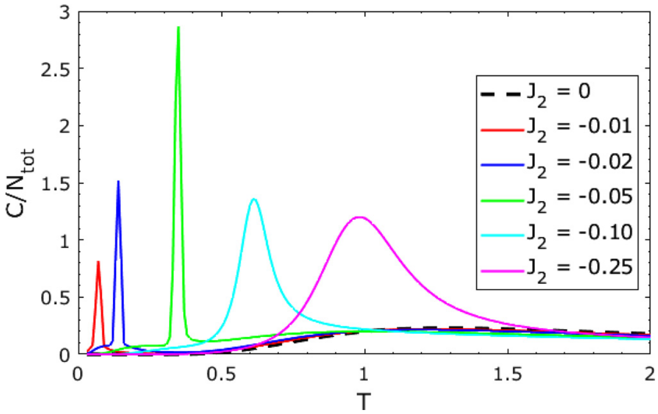

FIG. 2. Specific heat as a function of temperature for six different values of J_2, obtained from our $S(T)$ calculation. Peaks in the specific heat occur at temperatures at which the corresponding $S(T)$ curve sharply drops to zero.

to locate the amount of the entropy jump at the transition and the transition temperature for $J_2 = -0.1$. These are indicated in the inset figure by a dashed curve. Previous Monte Carlo data [45] are only available for a magnitude of J_2 greater than or equal to 0.1, which pushes the first-order transition temperature outside the plateau region of the nearest-neighbor model. Thus, we have developed further Monte Carlo simulations for $J_2 = -0.05$ and -0.02 (and also verified the results for $J_2 = -0.1$ [45]) to study the entropy jump at a temperature in the plateau region of the nearest-neighbor model. These jumps are also shown in the inset. The data are consistent with the absence of an entropy plateau for $|J_2| \geqslant 0.05$. For $J_2 = -0.02$, we calculate an entropy jump that is consistent with the sharp change in the entropy function observed below the plateau.

The specific heat per site is found using the relation $C = T\frac{\partial S}{\partial T}$, and is shown in Fig. 2 for a range of J_2 values. For nonzero values of J_2, a peak in the specific heat is observed at the temperature where $S(T)$ sharply drops, indicating a transition to an ordered ground state. The $J_2 = 0$ specific-heat curve (shown in black) has no peak, since ordering to a nondegenerate ground state does not occur. As

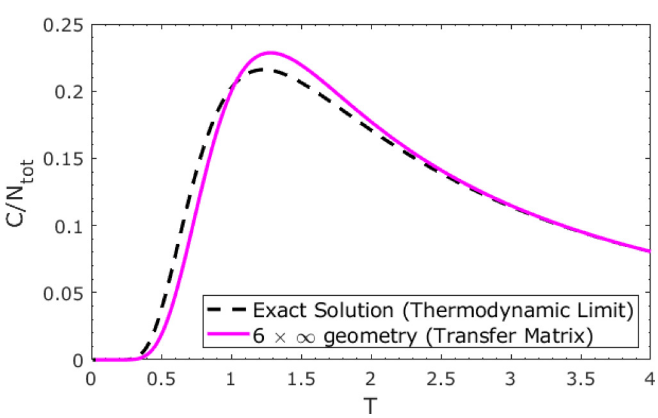

FIG. 3. Comparison of $C(T)$ calculated using the transfer-matrix method for our semi-infinite $6 \times \infty$ lattice with the exact result for the TIAF in the thermodynamic limit.

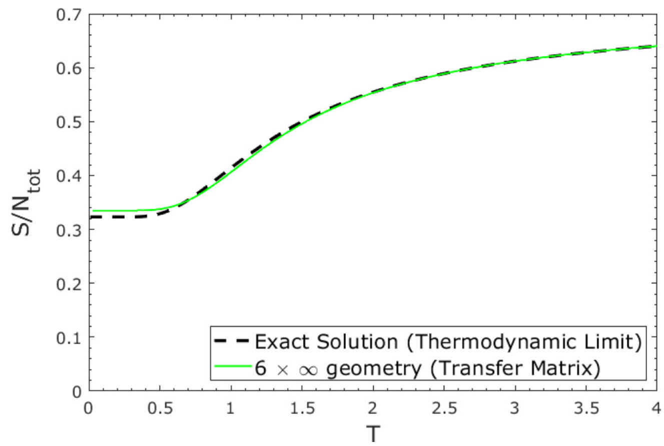

FIG. 4. Comparison of $S(T)$ with the exact result in the thermodynamic limit. We obtain a residual entropy of $S(0) \approx 0.3350$ for our semi-infinite $6 \times \infty$ lattice, which is slightly greater than the exact value $S(0) \approx 0.323\,06$ in the thermodynamic limit.

the magnitude of J_2 increases, the peaks in the specific heat are shifted to higher temperature, consistent with Fig. 1.

The entropy and specific heat of the infinite triangular lattice (i.e., in the thermodynamic limit) were calculated exactly by Wannier [34,35]. An exact expression for $C(T)$ (with NN interactions only) for the TIAF is given in [50], which is plotted in Fig. 3. The transfer-matrix result for $C(T)$ for our semi-infinite $6 \times \infty$ system is plotted for comparison, indicating our results are in good agreement with the exact case in the thermodynamic limit. By integrating the specific heat, we also obtain the exact form of $S(T)$ in the thermodynamic limit, which is shown in Fig. 4. The numerical result for $S(T)$ for our semi-infinite geometry is also shown, and the agreement between the numerical and exact results is even closer than it is for specific heat. The Wannier value of the residual entropy in the thermodynamic limit is $S(0) \approx 0.323\,06$ [35], and for our semi-infinite $6 \times \infty$ system we obtain $S(0) \approx 0.3350$.

B. Results in zero field with Gaussian disorder

We observe in Fig. 1 that in the absence of NNN interactions, $S(T)$ tends toward the residual entropy value as the temperature is reduced to zero, with a short plateau appearing at low temperature. With a nonzero J_2, we find that a plateau at the residual entropy value exists for a finite-temperature window, before $S(T)$ drops to zero. As the magnitude of J_2 increases (i.e., for $|J_2| \geqslant 0.05$) this plateau weakens, and we observe the $S(T)$ curve smoothly decreasing to zero. To determine the robustness of such entropy plateaus, we now consider the effect of Gaussian disorder (in the nearest-neighbor variable J_1) on the form of the $S(T)$ curve. Figure 5(a) shows the effect of increasing levels of Gaussian disorder in J_1 in the absence of next-nearest-neighbor interactions. To obtain $S(T)$ values with disorder, the trace of the product of 101 transfer matrices was taken, each one containing J_1 values drawn from a Gaussian distribution for each occurrence, i.e., each individual NN coupling in the lattice has a randomly chosen interaction strength. The particular set

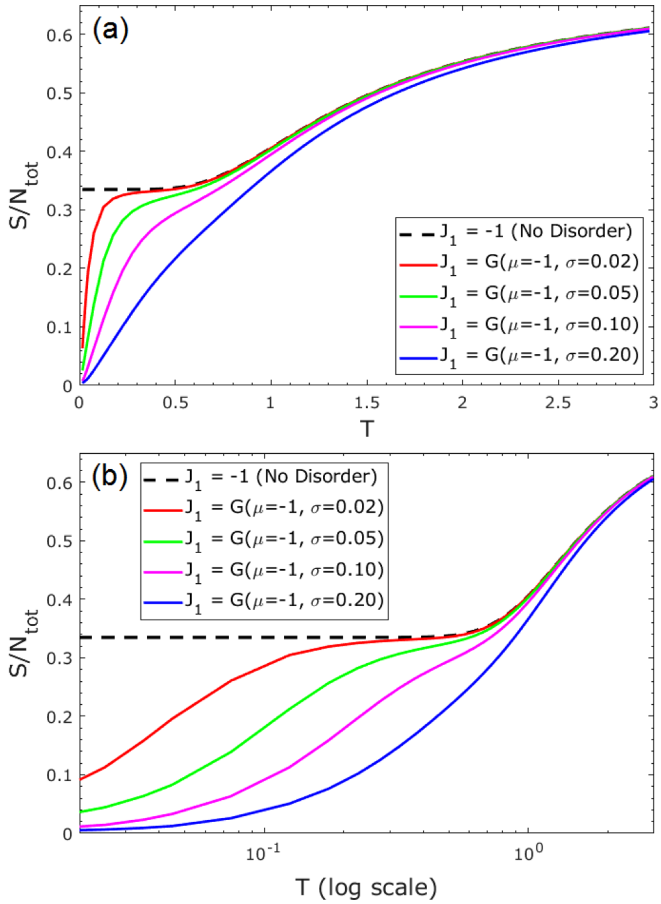

FIG. 5. (a) $S(T)$ results with Gaussian disorder in J_1 are shown for various values of σ, with $J_2 = 0$. The mean of the distribution is fixed at $\mu = -1$ in each case. The entropy curve in the absence of disorder is shown in black for comparison. (b) The same $S(T)$ results as above shown on a logarithmic temperature scale, emphasizing differences in plateau rounding at low T.

of J_1 values used was stored and used for each temperature increment.

We label Gaussian distributions by $G(\mu, \sigma)$, where μ and σ denote the mean and standard deviation, respectively. As σ is increased, the plateau at the value of the residual entropy is gradually weakened, and we eventually observe the $S(T)$ curve approaching zero with no plateau. At all temperatures, the entropy per site is lower for increasing levels of disorder, and we also find that for relatively low levels of disorder [e.g., $J_1 = G(-1, 0.02)$] an entropy plateau persists to quite low temperatures ($T \approx 0.2$). A logarithmic temperature scale emphasizes the influence of σ on the form of the entropy plateau at low values of T, as illustrated in Fig. 5(b). For wider distributions (i.e., $\sigma \geqslant 0.05$), a short plateau is no longer observed. Even in the absence of a NNN interaction, we see that the introduction of any amount of disorder in J_1 leads to a nondegenerate ground state with $S(T)$ approaching zero at $T = 0$. Moreover, the presence of weak disorder, i.e., with a standard deviation of just a few percent of the mean J_1 value, is enough to remove any sign of a plateau at low temperatures. This suggests that for the TIAF system, the existence of entropy plateaus is highly sensitive to disorder in the nearest-neighbor interaction.

C. Results in magnetic field with no disorder

Introducing a magnetic field aligned parallel to the Ising axis, the Hamiltonian given by Eq. (1) now has a nonzero value of B in the final term. Using the same transfer-matrix procedure with this Hamiltonian, we again obtained $S(T)$ and $C(T)$ plots at different values of B for various values of J_2. Figure 6 shows $S(T)$ for three NNN interaction strengths: (a) $J_2 = 0$, (b) $J_2 = -0.01$, and (c) $J_2 = -0.10$. For the

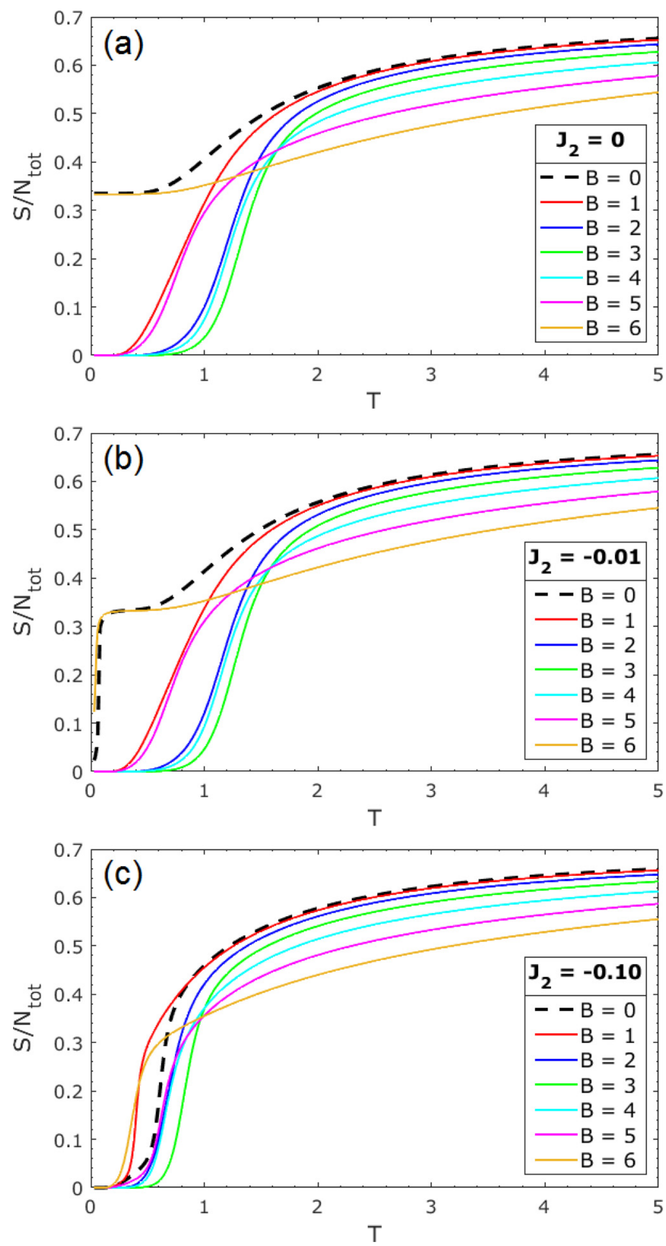

FIG. 6. $S(T)$ results in the presence of a magnetic field, with no disorder. Field strengths ranging from $B = 0$ to the TIAF critical field value $B_c = 6$ are shown. The magnitude of the NN interaction strength J_1 is set to 1. Entropy curves are shown for three different J_2 values: (a) $J_2 = 0$, (b) $J_2 = -0.01$, and (c) $J_2 = -0.10$.

$J_2 = 0$ case, we again find that for $B = 0$, we have a nonzero residual entropy as the temperature tends to zero. As noted in [43], a critical field value exists for antiferromagnetic Ising lattices at $B_c = z|J_1|$, at which there is degeneracy in the ground state. Here $z = 6$ for the triangular lattice, and we take $|J_1| = 1$. Hence we observe a nonzero residual entropy again at $B = 6$. For all other magnetic-field values, the entropy tends to zero at low temperature since the ground-state degeneracy due to frustration is removed.

When a NNN interaction is introduced, as in Fig. 6(b), where $J_2 = -0.01$, there is no residual entropy even at $B = 0$ or 6, since the ground-state degeneracy is removed. For small values of J_2 we observe a rounded plateau in $S(T)$ for $B = 0$ and 6. As the magnitude of J_2 increases, we no longer observe a plateau, and the entropy per site smoothly falls from $\ln 2$ to zero as the temperature is lowered. As in the previous section, plots of the specific heat (at various magnetic-field values) were obtained for $J_2 = 0$, -0.01, and -0.10, as shown in Figs. 7(a)–7(c). Comparing the $B = 0$ case in Figs. 7(a) and 7(b), we see that introducing a small nonzero NNN interaction (i.e., $J_2 = -0.01$) produces a peak in the specific heat, indicating a transition to a nondegenerate ground state and the absence of residual entropy at $T = 0$. Similarly, we also observe a peak in $C(T)$ at low temperature

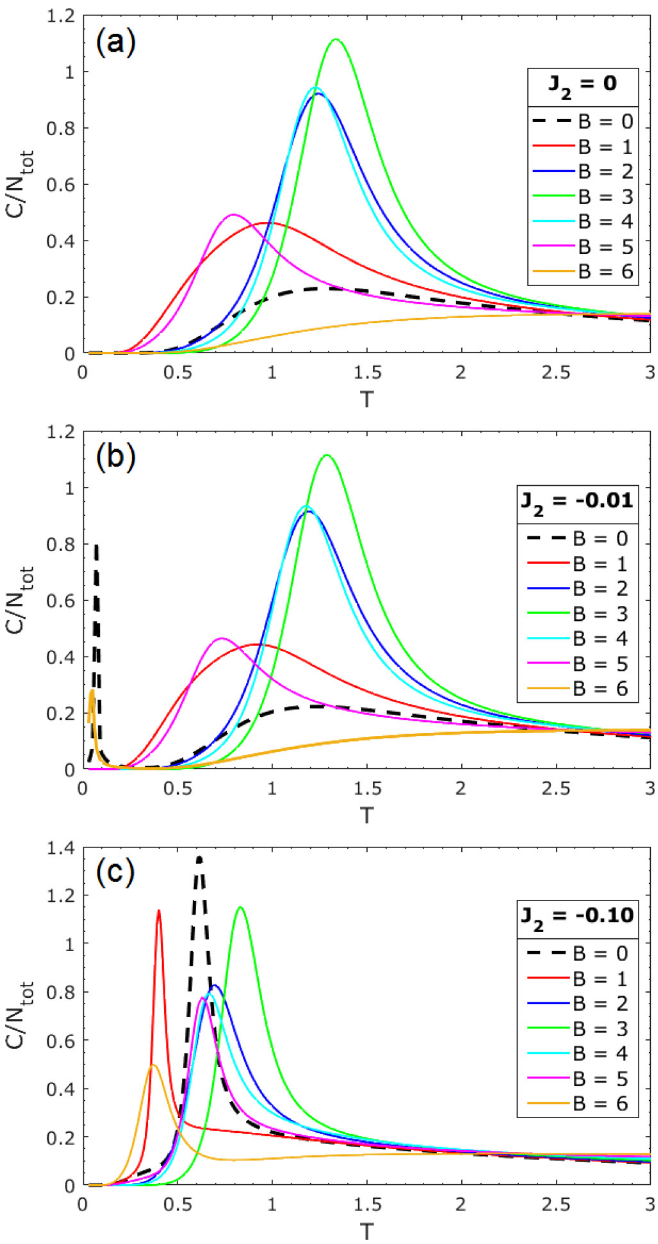

FIG. 7. $C(T)$ results in the presence of a magnetic field, with no disorder. Specific-heat curves are shown for three different J_2 values: (a) $J_2 = 0$, (b) $J_2 = -0.01$, and (c) $J_2 = -0.10$. Low-temperature peaks in $C(T)$ are observed for both $B = 0$ and $B = 6$ when there is a small NNN interaction present, i.e., for $J_2 = -0.01$.

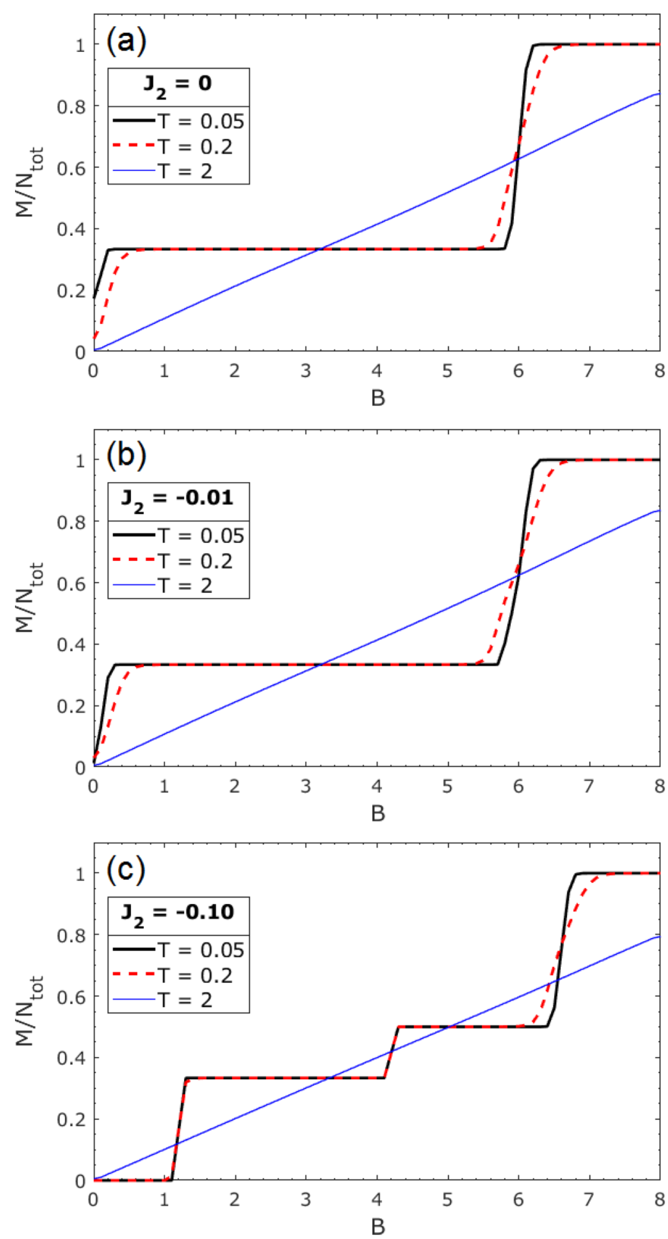

FIG. 8. $M(B)$ results at finite temperature for different values of J_2: (a) $J_2 = 0$, (b) $J_2 = -0.01$, and (c) $J_2 = -0.10$, without disorder. For $J_2 = -0.10$, steplike magnetization plateaus can be seen at both $M = 1/3$ and $1/2$. In each plot, $M(B)$ curves for three different temperatures are shown: $T = 0.05$, 0.2, and 2.

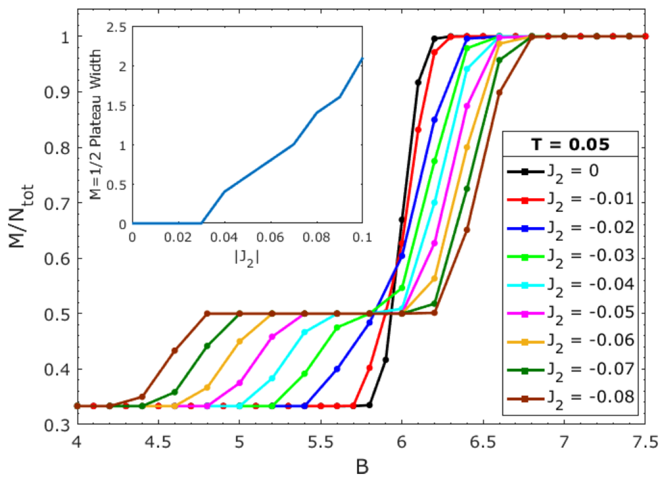

FIG. 9. $M(B)$ curves around the $M = 1/2$ plateau region are shown for various values of J_2 at a fixed finite temperature of $T = 0.05$. The inset graph shows the dependence of the $M = 1/2$ plateau width (in units of B) upon the magnitude of J_2.

for $B = 6$, when $J_2 = -0.01$. Increasing the magnitude of J_2 further, we find that the locations of the peaks are shifted to lower temperature for all values of B between $B = 0$ and 6.

With a nonzero magnetic field, we can obtain free energies at a fixed temperature for a range of B values and obtain the magnetization (per site) using $M = -\frac{\partial F}{\partial B}$. $M(B)$ curves were obtained at $T = 0.05$, 0.2, and 2 for three different values of J_2, as shown in Fig. 8: (a) $J_2 = 0$, (b) $J_2 = -0.01$, and (c) $J_2 = -0.10$. We find that at relatively high temperature (i.e., $T = 2$), magnetization per site increases linearly with magnetic field, and no plateaus occur. As temperature is lowered, magnetization plateaus are observed. The plateaus become less rounded and more steplike as the temperature is lowered further. For $J_2 = 0$ and -0.01, a single plateau is observed at $M = 1/3$, but for $J_2 = -0.1$ we observe another plateau at $M = 1/2$, suggesting the $M = 1/2$ plateau phase is only observed if the NNN interaction is sufficiently strong. Indeed, the J_2 dependence of the width of the $M = 1/2$ plateau at finite temperature (shown in Fig. 9) illustrates that a well-defined plateau appears only when $|J_2|$ exceeds some threshold value, with plateau width increasing approximately linearly with $|J_2|$ thereafter. At a temperature of $T = 0.05$, a plateau at $M = 1/2$ is apparent for $|J_2| \geqslant 0.04$. Decreasing the magnitude of J_2 gradually rounds the plateau until it is no longer present, and the magnetization per site increases smoothly from 1/3 to full saturation. From Fig. 8(c) we can see that for $J_2 = -0.10$ (at $T = 0.2$), we have an $M = 0$ stripe phase for approximately $0 < B < 1$, an $M = 1/3$ plateau phase in the region $1.2 < B < 4.1$, and an $M = 1/2$ phase for $4.2 < B < 6$. Greater values of magnetic field produce a fully spin-polarized phase with $M = 1$. We also find that as the temperature increases, the rounding of the $M = 1/2$ plateau is more pronounced than at $M = 1/3$, which at $J_2 = -0.10$ and $T = 0.2$ remains steplike, as shown in Fig. 8(c) (red curve).

D. Results in magnetic field with uniform and Gaussian disorder

Although rounding of the magnetization plateaus in the ideal TIAF system is illustrated here at finite temperature, at $T = 0$ the magnetization per site increases in discrete steps between 0, 1/3, 1/2, and 1. However, in low-temperature measurements of TIAF materials such as $TmMgGaO_4$ [38,39], distinct plateaus in magnetization are absent, which has been ascribed to the presence of disorder in intersite interactions and coupling to the magnetic field, which weakens or removes these plateaus entirely. The influence of disorder on $M(B)$ for the TIAF with both NN and NNN interactions has been studied previously for a finite 6×6 cluster by Li *et al.* [39], where it was found that introducing disorder produced magnetization curves in agreement with experiment. Motivated by this work, we studied the influence of disorder strength on the form of the magnetization plateaus, and we also investigated the relative importance of disorder in J_1 and J_2.

Using the transfer-matrix approach to obtain $M(B)$, one introduces disorder in J_1 and J_2 by generating random values of these parameters from a chosen distribution. For a given set of J_1 and J_2 values (for all individual NN and NNN couplings in the lattice), we produce the corresponding transfer matrices as before, however the partition function is now obtained by taking the trace of the product of P transfer matrices, each one containing different parameter values. We use $P = 101$ and parameter values drawn from both a uniform distribution and a Gaussian distribution in the results presented here, with temperature fixed at $T = 0.2$. Uniform distributions

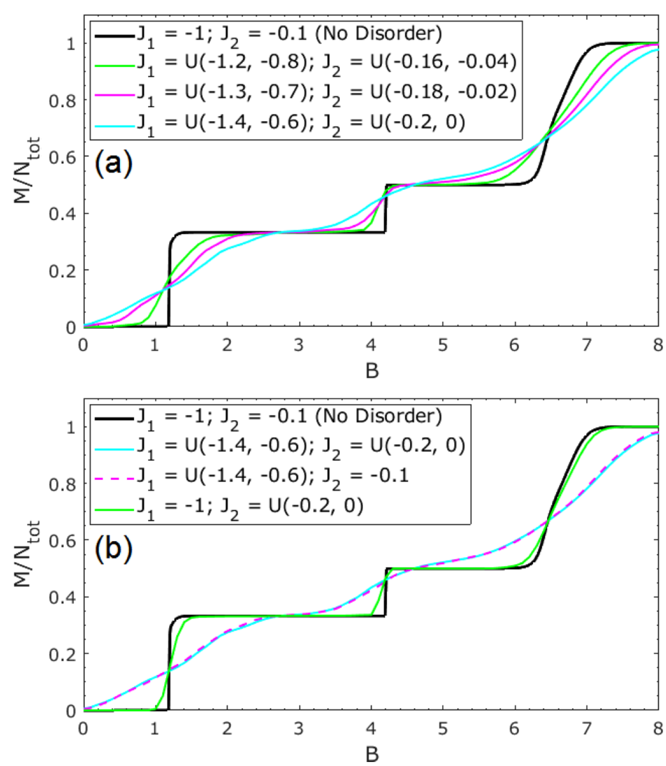

FIG. 10. (a) $M(B)$ results for three different levels of uniform disorder, in both J_1 and J_2 combined, with the zero-disorder result shown in black for comparison. In each case, the uniform distributions of J_1 and J_2 used are centered at -1 and -0.1, respectively. (b) Additional $M(B)$ results are shown for uniform disorder in J_1 only [$J_1 = U(-1.4, -0.6)$ with $J_2 = -0.1$] and in J_2 only [$J_2 = U(-0.2, 0)$ with $J_1 = -1$].

are denoted by $U(J_{\min}, J_{\max})$, where $J_{\min}$ and $J_{\max}$ are the boundaries of the distribution, which has a width $J_{\max} - J_{\min}$. As shown in Fig. 10(a), we observe that strong plateaus at both $M = 1/3$ and $1/2$ remain for $J_1 = U(-1.2, -0.8)$ and $J_2 = U(-0.16, -0.04)$, i.e., uniform distributions with mean values of $J_1 = -1$ and $J_2 = -0.1$. As the distribution width is increased, the plateaus are rounded further, and we find that both the $M = 1/2$ and $1/3$ plateaus are eventually no longer observable, e.g., for $J_1 = U(-1.4, -0.6)$ and $J_2 = U(-0.2, 0)$. There is an indication that the $M = 1/3$ plateau may be more robust to disorder than the $M = 1/2$ plateau, since as the level of disorder increases, the plateau at $M = 1/2$ is lifted while a short plateau remains observable at $M = 1/3$, which can be seen for $J_1 = U(-1.3, -0.7)$ and $J_2 = U(-0.18, -0.02)$. When the disorder strength is increased further [i.e., to $J_1 = U(-1.4, -0.6)$ and $J_2 = U(-0.2, 0)$], the weak plateau at $M = 1/3$ is no longer present, and one obtains a magnetization curve quite similar to the recent experimental result for $TmMgGaO_4$ [39].

We also investigated introducing disorder in only one of the parameters J_1 or J_2 as shown in Fig. 10(b), using uniform distributions $J_1 = U(-1.4, -0.6)$ and $J_2 = U(-0.2, 0)$, again with mean values $J_1 = -1$ and $J_2 = -0.1$. We find that with disorder in J_2 only, both plateaus at $M = 1/3$ and $1/2$ are present, and the magnetization curve remains similar to the zero-disorder case. With disorder in J_1 only, both plateaus are completely removed, and $M(B)$ is essentially identical to our result with disorder in both J_1 and J_2 combined. This suggests that disorder in J_1 is only sufficient to eliminate both magnetization plateaus, giving an $M(B)$ curve similar to experiment, provided $|J_1|$ exceeds $|J_2|$ by approximately an order of magnitude, as in this study. In this case, magnetization plateaus in the TIAF system are robust to disorder solely in J_2, even when the width of the parameter distribution spans $\pm 100\%$ of the mean value, i.e., for $J_2 = U(-0.2, 0)$. With disorder in J_2 only, steplike transitions between magnetization plateaus are still present, and there is only a slight rounding of the magnetization curve compared to the zero-disorder case, even for $J_2 = U(-0.2, 0)$. We also find that disorder in the magnetic field is relatively insignificant, and one can obtain a result qualitatively similar to experiment with disorder in J_1 and J_2 only.

The form of the $M(B)$ curves in the presence of Gaussian disorder in J_1 and J_2 (instead of uniform disorder) was also investigated, as shown in Fig. 11. The Gaussian distributions for J_1 and J_2 were chosen to have mean values of -1 and -0.1, respectively, with the standard deviation of the distribution of J_2 values fixed at $\sigma = 0.1/\sqrt{3}$. The width of the distribution of J_1 values was varied and $M(B)$ results compared to the zero-disorder case. Three Gaussian distributions were used, which were chosen to have the same standard deviations for J_1 as the three uniform distributions shown in Fig. 10(a), where we have used $\sigma = (b - a)/\sqrt{12}$ for any uniform distribution $U(a, b)$. As with uniform disorder, increasing the width of the distribution gradually weakens the magnetization plateaus at $M = 1/3$ and $1/2$ until both are no longer visible, which occurs when the standard deviation of J_1 values approaches $\sigma = 0.4/\sqrt{3}$. The strong similarity between our results for uniform and Gaussian disorder indicates that the exact form of the distribution used is relatively unimportant in determining the robustness of magnetization plateaus in the TIAF system.

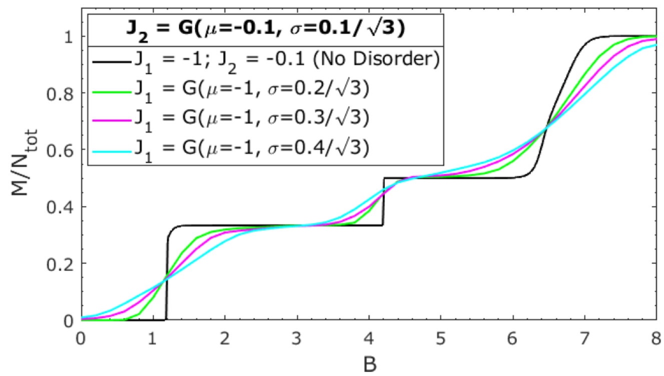

FIG. 11. $M(B)$ results for three different levels of Gaussian disorder, in both J_1 and J_2 combined, with the zero-disorder result shown in black for comparison. The standard deviations of the distributions of J_1 values match those used in Fig. 10(a) for the case of uniform disorder.

IV. SUMMARY AND CONCLUSIONS

In this work, we have studied the rounding and in some cases complete absence of entropy and magnetization plateaus for the triangular lattice antiferromagnet, with both NN and NNN interactions in a magnetic field, with and without quenched disorder. In particular, we have found that in the ideal TIAF, increasing $|J_2|$ tends to round and quickly remove the plateau in $S(T)$ near the theoretical residual entropy value at low temperature. The plateaulike feature is replaced by a sharp drop in entropy at the first-order transition. The strength of the second-nearest-neighbor interaction also determines if a magnetization plateau at $M = 1/2$ is present at finite temperature, and controls the width of the plateau. For sufficiently large J_2, a distinct plateau at $M = 1/2$ will be visible, which is gradually rounded as the magnitude of J_2 is lowered, until a plateau no longer remains.

To model realistic TIAF materials such as $TmMgGaO_4$, we studied the influence of disorder in J_1 and J_2 on the form of the entropy and magnetization curves. We find that with nearest-neighbor interactions alone, rounded entropy plateaus are quite sensitive to disorder in the exchange variable, and they are no longer observed when the width of the J_1 distribution exceeds $\sigma \approx 0.05 J_1$. For weaker levels of disorder, a plateau at the residual entropy value persists to low temperatures (around $T = 0.2$ for $\sigma = 0.02 J_1$). Consequently, we expect rounded entropy plateaus to be observable in TIAF systems at low temperatures only if the second-neighbor interactions are less than a few percent and there is a significant absence of quenched disorder in the system. Our $M(B)$ results with disorder are close to recent experimental observations [39], confirming the presence of second-neighbor interactions and disorder in the system.

More generally, we conclude that the existence of well-defined entropy plateaus requires a fair amount of fine-tuning of the system, so whether they will be observed in a generic frustrated magnet is unclear. The spin-ice system is clearly special. The fact that a residual entropy plateau is seen in model simulations with arbitrary strength long-range dipolar interactions in addition to nearest-neighbor exchange interactions [3–5] shows their robustness. One might have expected these long-range interactions to remove the ground-state degeneracy and the corresponding zero-point entropy. But, it has been shown that a "model dipole" interaction can be constructed that has exactly the same ground states as the nearest-neighbor model [51,52]. Remarkably, the dipolar interaction on the pyrochlore lattice has the noteworthy property of differing only slightly from this model interaction, and at short distances only. This robustness is presumably a manifestation of the emergent gauge theory.

Independent of the issue of fine-tuning, there are strong experimental challenges in looking for these entropy plateaus in real materials. The need to have clean low-disorder material and to be able to isolate the magnetic contribution to heat capacity and entropy from phonons and other degrees of freedom can be formidable. We hope our work will motivate further work on entropy plateaus in frustrated magnets and also in strongly correlated electron systems, where a residual entropy phase may be a precursor to intertwined and competing orders [53].

ACKNOWLEDGMENTS

The authors thank W. Pickett for useful discussions. This work is supported in part by DOE Grants No. DE-SC0014671 (R.T.S.) and No. DE-FG02-04ER46111 (O.B. and C.F.) and by the U.S. National Science Foundation DMR Grant No. 1855111 (R.R.P.S.).

[1] L. Balents, Nature (London) **464**, 199 (2010).
[2] L. Pauling, J. Am. Chem. Soc. **57**, 2680 (1935).
[3] B. C. den Hertog and M. J. P. Gingras, Phys. Rev. Lett. **84**, 3430 (2000); R. G. Melko, B. C. den Hertog, and M. J. P. Gingras, *ibid.* **87**, 067203 (2001).
[4] C. Castelnovo, R. Moessner, and S. L. Sondhi, Nature (London) **451**, 42 (2008).
[5] J. S. Gardner, M. J. P. Gingras, and J. E. Greedan, Rev. Mod. Phys. **82**, 53 (2010).
[6] A. P. Ramirez, A. Hayashi, R. J. Cava, R. Siddharthan, and B. S. Shastry, Nature (London) **399**, 333 (1999).
[7] X. Ke, R. S. Freitas, B. G. Ueland, G. C. Lau, M. L. Dahlberg, R. J. Cava, R. Moessner, and P. Schiffer, Phys. Rev. Lett. **99**, 137203 (2007).
[8] A. L. Cornelius and J. S. Gardner, Phys. Rev. B **64**, 060406(R) (2001).
[9] See *Introduction to Frustrated Magnetism: Materials, Experiments, Theory*, edited by C. Lacroix, P. Mendels, and F. Mila, Springer Series in Solid State Sciences (Springer, London, 2011).
[10] G. Jackeli and G. Khaliullin, Phys. Rev. Lett. **102**, 017205 (2009).
[11] J. G. Rau, EricKin-Ho Lee, and H.-Y. Kee, Phys. Rev. Lett. **112**, 077204 (2014).
[12] S. M. Winter, A. A. Tsirlin, M. Daghofer, J. van den Brink, Y. Singh, P. Gegenwart, and R. Valenti, Top. Rev. J. Phys.: Condens. Matter **29**, 493002 (2017).
[13] R. Sano, Y. Kato, and Y. Motome, Phys. Rev. B **97**, 014408 (2018).
[14] Y. Singh, S. Manni, J. Reuther, T. Berlijn, R. Thomale, W. Ku, S. Trebst, and P. Gegenwart, Phys. Rev. Lett. **108**, 127203 (2012).
[15] A. Kitaev, Ann. Phys. (NY) **321**, 2 (2006).
[16] J. Nasu, M. Udagawa, and Y. Motome, Phys. Rev. B **92**, 115122 (2015); J. Nasu, J. Yoshitake, and Y. Motome, Phys. Rev. Lett. **119**, 127204 (2017).
[17] S.-H. Do, S.-Y. Park, J. Yoshitake, J. Nasu, Y. Motome, Y. S. Kwon, D. T. Adroja, D. J. Voneshen, K. Kim, T.-H. Jang, J.-H. Park, K.-Y. Choi, and S. Ji, Nat. Phys. **13**, 1079 (2017).
[18] Y. Wang, G. B. Osterhoudt, Y. Tian, P. Lampen-Kelley, A. Banerjee, T. Goldstein, J. Yan, J. Knolle, J. Nasu, Y. Motome, S. Nagler, D. Mandrus, and K. S. Burch, arXiv:1809.07782.
[19] G. Baskaran, D. Sen, and R. Shankar, Phys. Rev. B **78**, 115116 (2008).
[20] S. Chandra, K. Ramola, and D. Dhar, Phys. Rev. E **82**, 031113 (2010).
[21] A. Koga, H. Tomishige, and J. Nasu, J. Phys. Soc. Jpn. **87**, 063703 (2018).
[22] J. Oitmaa, A. Koga, and R. R. P. Singh, Phys. Rev. B **98**, 214404 (2018).
[23] L. De Leo, J.-S. Bernier, C. Kollath, A. Georges, and V. W. Scarola, Phys. Rev. A **83**, 023606 (2011).
[24] G. Li, A. E. Antipov, A. N. Rubtsov, S. Kirchner, and W. Hanke, Phys. Rev. B **89**, 161118(R) (2014).
[25] T. Paiva, R. T. Scalettar, C. Huscroft, and A. K. McMahan, Phys. Rev. B **63**, 125116 (2001).
[26] G. Jütner, A. Klümper, and J. Suzuki, Nucl. Phys. B **522**, 471 (1998).
[27] H. Shiba and P. A. Pincus, Phys. Rev. B **5**, 1966 (1972).
[28] J. Schulte and M. C. Böhm, Phys. Rev. B **53**, 15385 (1996).
[29] A. Georges and W. Krauth, Phys. Rev. B **48**, 7167 (1993).
[30] D. Vollhardt, Phys. Rev. Lett. **78**, 1307 (1997).
[31] N. Chandra, M. Kollar, and D. Vollhardt, Phys. Rev. B **59**, 10541 (1999).
[32] B. Tang, T. Paiva, E. Khatami, and M. Rigol, Phys. Rev. B **88**, 125127 (2013).
[33] S. Sorella, Y. Otsuka, and S. Yunoki, Sci. Rep. **2**, 992 (2012).
[34] G. H. Wannier, Phys. Rev. **79**, 357 (1950).
[35] G. H. Wannier, Phys. Rev. B **7**, 5017 (1973).
[36] Y. Q. Liu, S. J. Zhang, J. L. Lv, S. K. Su, T. Dong, G. Chen, and N. L. Wang, arXiv:1612.03720.
[37] K. Katsumata, H. A. Katori, S. Kimura, Y. Narumi, M. Hagiwara, and K. Kindo, Phys. Rev. B **82**, 104402 (2010).
[38] F. A. Cevallos, K. Stolze, T. Kong, and R. J. Cava, Mater. Res. Bull. **105**, 154 (2018).
[39] Y. Li, S. Bachus, Y. Tokiwa, A. A. Tsirlin, and P. Gegenwart, arXiv:1804.00696.
[40] B. D. Metcalf, Phys. Lett. A **45**, 1 (1973).
[41] W. Kinzel and M. Schick, Phys. Rev. B **23**, 3435 (1981).
[42] B. D. Metcalf, Phys. Lett. A **46**, 325 (1974).
[43] B. D. Metcalf and C. P. Yang, Phys. Rev. B **18**, 2304 (1978).
[44] C.-O. Hwang, S.-Y. Kim, D. Kang, and J. M. Kim, J. Kor. Phys. Soc. **52**, 203 (2008).

[45] E. Rastelli, S. Regina, and A. Tassi, Phys. Rev. B **71**, 174406 (2005).

[46] L. Gu, B. Chakraborty, P. L. Garrido, M. Phani, and J. L. Lebowitz, Phys. Rev. B **53**, 11985 (1996).

[47] L. Kurbah, D. Thongjaomayum, and P. Shukla, Phys. Rev. E **91**, 012131 (2015).

[48] M. Žukovič, M. Borovský, and A. Bobák, Phys. Lett. A **374**, 4260 (2010).

[49] R. Applegate, N. R. Hayre, R. R. P. Singh, T. Lin, A. G. R. Day, and M. J. P. Gingras, Phys. Rev. Lett. **109**, 097205 (2012); N. R. Hayre, K. A. Ross, R. Applegate, T. Lin, R. R. P. Singh, B. D. Gaulin, and M. J. P. Gingras, Phys. Rev. B **87**, 184423 (2013).

[50] B. D. Metcalf, Ph.D. thesis, The Ohio State University, 1974.

[51] S. V. Isakov, R. Moessner, and S. L. Sondhi, Phys. Rev. Lett. **95**, 217201 (2005).

[52] C. Castelnovo, R. Moessner, and S. L. Sondhi, Annu. Rev. Condens. Matter **3**, 35 (2012).

[53] E. Fradkin, S. A. Kivelson, and J. M. Tranquada, Rev. Mod. Phys. **87**, 457 (2015).